L-band Radars Using a Large Deployable Antenna for Measurements of Soil Moisture and Ice Shelves Melt Rates, and Sounding and Imaging of Ice Sheets in Antarctica and Greenland

Sivaprasad Gogineni*, Jie Yan, Charles O'Neill, Richard Branam,

College of Engineering, The University of Alabama, Tuscaloosa, AL

David Braaten, *CReSIS, The University of Kansas, Lawrence, KS*

Ian Joughin, *Applied Physics Lab, University of Washington, Seattle, WA*

Mahta Moghaddam, *University of Southern California, CA*

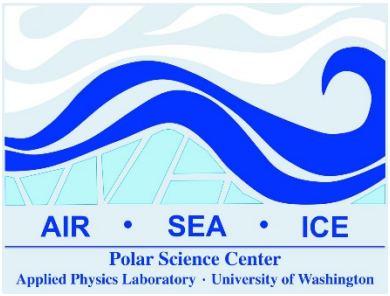

Technical Report
CReSIS TR 165

November 2, 2016

*Now with CReSIS at The University of Kansas and with The University of Alabama from January 2017

1.0 Introduction

As atmospheric and oceanic warming proceeds, increased evaporation rates, changing precipitation patterns and extreme, prolonged drought, and dramatic cryosphere changes are creating a new paradigm that will impact society's interaction with the water cycle and retreating coastal zones caused by sea-level rise. Population and economic growth are fueling demands for increased water resources and at the same time are increasingly vulnerable to extreme floods, droughts, and heat waves that are predicted to occur more frequently in a warming climate [IPCC, 2014; Zhao, T. and A. Dai, 2015; Smith et al., 2013]. In 2016, these extreme events have resulted in significant losses in property, infrastructure, and economic activity that are in the tens of billions of dollars [NOAA, 2016]. To manage limited and variable water resources in a way that minimizes disruption, as well as forecasting, monitoring, and managing extreme events to protect the public requires large-scale measurements of rainfall, seasonal snow, soil moisture, and water storage in reservoirs, rivers and subsurface aquifers. Large-scale measurements of polar ice sheets are also critically needed to understand and manage a relentlessly expanding coastal inundation due to sea-level rise. These large-scale measurements are most effectively obtained with satellites equipped with appropriate sensors. Because of its links to evaporation and rainfall runoff, a key variable for managing water resources and forecasting floods and droughts is soil moisture. Knowledge of soil moisture conditions is also important to managing water usage in agriculture and for advancing precision-agriculture techniques. These data needs have long been acknowledged, and in January 2015 NASA launched the Soil Moisture Active Passive (SMAP) satellite. This satellite was equipped with an L-band radar and a radiometer to map soil moisture and freeze/thaw states [Entekhabi., et a., 2010; Entekhabi et al., 2014]. Unfortunately, the radar onboard SMAP prematurely failed in July 2015, delivering a major setback for fine-resolution large-scale measurements of soil moisture. While the radiometer continues to function, the inherent limitation of a spaceborne passive-microwave system is its poor resolution. This was the primary justification for including the radar on SMAP [Entekhabi et al, 2010, Moore and Gogineni 1984].

Sea level rise is beginning to have major social, economic and political impacts on the more than 100 million people that live within 1 m elevation of present sea level [Rowley et al., 2007; Li et al., 2009]. As sea level continues to increase, the number of coastal flooding events in many Atlantic coast communities is also increasing. IPCC has estimated that sea level will increase by about 26 cm at the minimum and 96 cm at the maximum under different warming scenarios by about 2100 [IPCC 2014]. As a caveat, the IPCC report acknowledges that uncertainties related to ice sheet contributions to sea level could mean that their sea-level rise estimates are substantially underestimated. A major unknown in sea-level rise projections is the contribution of large ice sheets particularly the one in Antarctica. Given that almost all megacities as well as critical infrastructure are located in coastal zones, a rapid and unexpected sea-level rise situation would have devastating consequences on our interdependent global society. Managing the social and economic impacts of sea-level rise will depend on our ability to accurately project the rate and extent of the rise over the next century, and implementing a decision-making triage to decide where to invest limited coastal protection resources.

The NASA Ice, Cloud, and land Elevation Satellite-2 (ICESat-2), and the NASA-ISRO Synthetic Aperture Radar (NISAR), each costing more than 1 billion dollars, are scheduled to be launched over the next few years. ICESat-2, scheduled to be launched in 2018, will focus on changes in the surface elevation of the ice sheets in both Greenland and Antarctica, providing an assessment

of mass balance changes [Abdalati, et al, 2010]. NISAR will measure surface velocities of both ice sheets [NISAR Workshop Report, 2014]. These satellites will provide complimentary information related to mass loss or gain, as well as changes in ice flux related to the speed-up or slow-down of outlet glaciers. Additional information on bed topography and basal conditions is needed for understanding current ice sheet behavior, as well as predicting the future state of the ice sheets that will enable accurate estimates of their contribution to sea-level rise. This critical information, in particular for the Antarctic Ice Sheet, can be obtained with satellite-based radars operating in the lower part of the L-band.

The development of an L-band radar with modest usable resolutions and near real-time processing capability is possible now because of the major technical advances in large (> 15 m) deployable antennas, RF & Microwave and high-speed digital systems. We can employ large bandwidth to obtain fine range resolution and Doppler beam sharpening to improve along-track resolution for producing small pixels within the antenna footprint. With the use of a large deployable reflector antenna, the radar power requirements are modest and Doppler beam sharpening can improve resolution in the along-track direction. Thus, improved resolution can be achieved with no increase in transmitter power and with a relatively simple processor.

Large deployable 15-30 m reflectors are currently developed and deployed to support military and civilian applications [Belvin, 2004]. Also large investments by the communication industry have contributed to major advances in RF & Microwave and high-speed digital components and systems. These technologies can be leveraged to develop compact multi-beam L-band radars to measure soil moisture over land. The same radar can be used to sound and image ice, and to measure the bottom melt rates of ice shelves and support other scientific and operational applications. In this report we present the feasibility for a satellite L-band radar with a large deployable antenna for ice sounding and imaging, and measuring bottom melt rates of ice shelves, measuring soil moisture over land and detecting freeze-thaw.

2.0 An L-band Radar for Soil Moisture and Cryosphere Studies

We propose to use L-band radar for spaceborne soil moisture measurements, and sounding and imaging of ice-sheets with a large 15-30 m antenna. The inclusion of an L-band radiometer on the satellite would substantially enhance the scientific value of the radar mission. The use of L-band radars and radiometers for soil moisture measurements has been demonstrated with airborne and spaceborne systems [Dubois et al. 1995; Shi et al. 1997; Entakabi et al, 2010; Kerr et al., 2012; Panciera, et al., 2014; Leroux et al., 2016]. The SMAP employed a 6-m antenna for synergistic use of radar and radiometer data to attain better results than possible with either alone. A microwave radiometer using the 15-m large-deployable will enhance radiometer resolution beyond that of the SMAP-radiometer by a factor of 2.5, thereby making passive microwave data much more useful.

The L-band radar and radiometer can provide very valuable information on polar ice sheets and ice shelves needed by models to generate more accurate estimates of ice sheets' contribution to sea level rise. We argue that an L-band radar can be used for sounding and imaging ice. Our concept is based on our previous success in sounding of 600-800 m thick ice in Antarctica and Greenland with a UHF radar, referred to as the accumulation radar, operating at a center frequency of 750 MHz with a bandwidth of 300 MHz, peak power of about 1 W and an antenna with gain of less than 10-dBi [Lewis, et al., 2015]. The L-band radiometer in conjunction with other

satellite passive data available from higher microwave frequency systems can be used to estimate ice temperature as a function of depth.

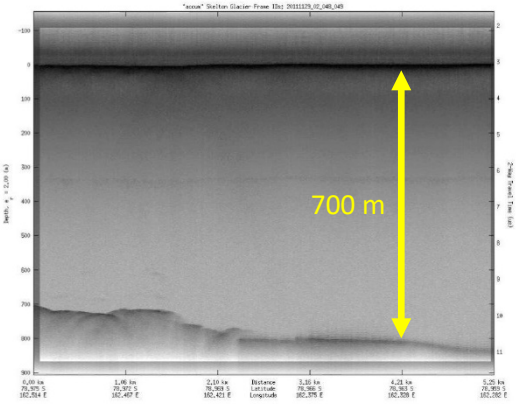

Figure 1: Accumulation radar data collected on ice near the Byrd Glacier.

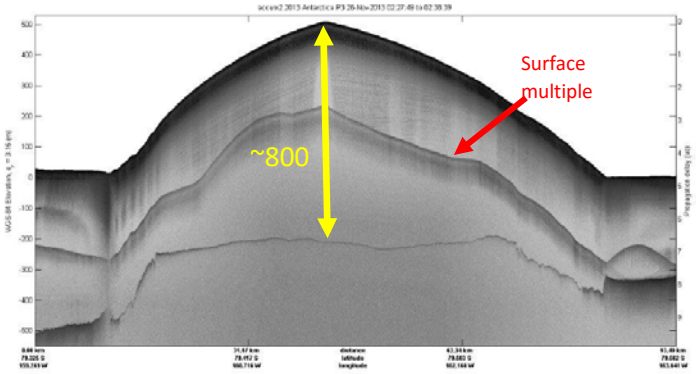

Figure 2: Accumulation-radar data collected on ice near Roosevelt Island in 2013.

Figure 1 and 2 show data collected with the accumulation radar on a Twin Otter aircraft on ice near the Byrd glacier and the NASA P-3 aircraft near Roosevelt Island, respectively. Since the radar was developed for collecting near-surface snow accumulation data, the digital-system was designed to collect data only up to a maximum ice thickness of about 700 m from an altitude of 500 m. Figure 2 shows accumulation-radar data collected with the system on the NASA P-3 aircraft in 2013. The maximum ice thickness is about 800 m with the aircraft flying at about 400 m above the surface.

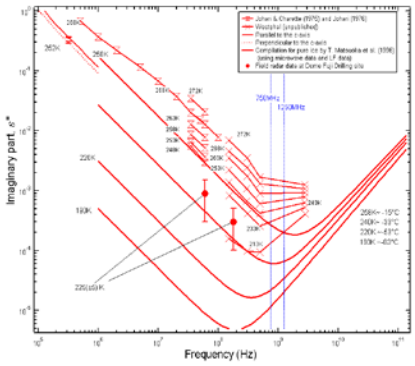

Figure 3: Imaginary part of the dielectric constant of ice [Fujita et la, 2000].

Figure 3 shows the imaginary part of the dielectric constant of Antarctic ice reported by Fujita et al. [2000]. The data show a broad null around 1.2 GHz. Using dielectric data in Fujita et al. [2000] and previous ice-sounding data collected with the accumulation radar, we estimated the one-way ice loss to be between 7.5 and 10 dB/km.

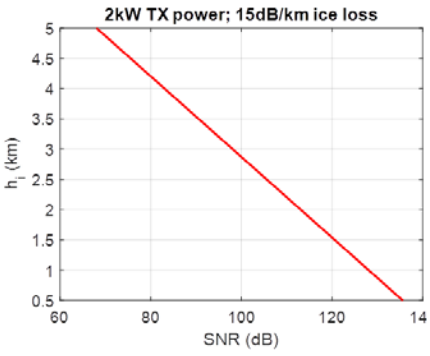

Figure 4: Estimated SNR for the L band radar on a satellite.

We computed signal-to-noise ratio (SNR) for a satellite-based L-band radar operating at 1.3 GHz with a peak transmit power of 2 kW, a 20-us long chirp pulse, and a bandwidth of 80 MHz.

The estimated SNR shown in Figure 4 indicates that we can sound close to 4-5 km thick low-loss ice in East Antarctica with an L-band radar operating with 2 kW peak power and antenna array with a gain of 45 dBi.

In addition to ice sounding, the L-band radar offers an enhanced sensitivity to detect the presence of water at the bed. Water layers on the order of 5-15 mm are speculated to exist under ice streams, and detection of such layers is critical to understanding ice dynamics as it serves as a critical boundary condition for ice-sheet

modeling [Weertman, 1957; Flowers, 2015]. The radar conceptual design also provides additional sensitivity to water layers as thin 1 mm as shown in Figure 5, assuming that we can discern frozen and wet beds with a 3-dB change in reflectivity. Our L-band radar would open a new era in ice sounding and imaging as well as for determining basal conditions unambiguously. The L-band radar can also measure bottom melt rates of ice shelves using repeat pass interferometry and tomography techniques [Lewis, 2015].

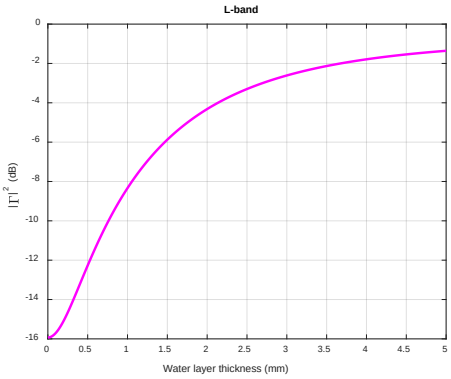

Figure 5: L-band radar sensitivity to detect the presence of water at the ice bed.

In summary, our analysis supports a major satellite mission can be developed to perform measurements of soil moisture globally over land and ice in Antarctica. This satellite can be developed using large-antenna technology, pioneered by U.S. DoD and Direct Broadcast Satellite (DBS) industries, and by taking advantage of advances made in RF & Microwave and digital areas because of the large investments made by the communication industry.

3.0 Radar and Antenna array design

In this section, we provide a brief summary of high-level radar design. We computed S/N ratio for about 1300 MHz both for planar and rough ice-bed interfaces and assumed that the ice is 5-km thick (an approximate upper limit for Antarctica) with 15 dB/km loss. The S/N ratio for a planar interface is given by

$$\frac{S}{N} = \frac{P_T G^2 \lambda^2 \left(1-|\Gamma_s|^2\right)^2 |\Gamma_{ib}|^2 C_I M}{(8\pi)^2 (h+d\sqrt{\varepsilon_r})^2 k T_{sys} B L_i} \quad (1)$$

Where P_T = transmit power in Watts; L_i = attenuation loss in ice; Γ_s = reflection coefficient at ice-air interface; Γ_{ib} = reflection coefficient at ice-bed interface; $C_I =$ pulse compression gain and $C_I = k\frac{T_u}{T_c}$ and k is a factor that accounts for transmit waveform shaping to reduce Fresnel ripples and weighting to reduce to sidelobes — normally k ~0..5; T_u = uncompressed pulse width; T_c = compressed pulse width, h = height of sensor above the surface = 600 km; d = ice thickness in km, $T_{sys} =$ system noise temperature and $T_{sys} = T_a + T_e$ with $T_a = \eta_a T_{sky} + (1-\eta_a)T_a$ and with T_e=Receiver noise temperature and $T_e = (F-1)T_o$. The coherent integration gain is given by, $M = 2\sqrt{\frac{(h+d\sqrt{\varepsilon_r})\lambda}{2}}\frac{f_p}{v}$; where f_p = pulse repetition frequency in Hz, v = spacecraft velocity in m/s, G = antenna gain and λ = wavelength. We assumed a pulse repetition frequency of 2500 Hz.

For rough ice-bed interface, neglecting refraction, the radar equation with SAR processing in the along-track direction is given by

$$\frac{S}{N} = \frac{P_T G^2 \lambda^2 \left(1-|\Gamma_s|^2\right)^2 \sigma^0 A C_I M}{(4\pi)^3 (h+d\sqrt{\varepsilon_r})^4 k T_{sys} B L_i} \quad (2)$$

where σ^0 = backscattering coefficient and A = illuminated area in m^2 and can be approximated as

$$A = 2\sqrt{c\tau(h + d\sqrt{\varepsilon_r})}\ \frac{(h+d\sqrt{\varepsilon_r})\lambda}{L_{eff}} = 2\sqrt{c\tau(h + d\sqrt{\varepsilon_r})}\ \frac{(h+d\sqrt{\varepsilon_r})\lambda}{vT_{in}} \quad (3)$$

Substituting for A in equation (2), we can obtain an expression S/N ratio for a rough interface as

$$\frac{S}{N} = \frac{2P_T G^2 \lambda^3 \left(1-|\Gamma_s|^2\right)^2 \sigma^0 \sqrt{c\tau}\, C_I M}{(4\pi)^3 (h+d\sqrt{\varepsilon_r})^{2.5} k T_{sys} B v T_{in} L_i} \quad (4)$$

We estimated our radar performance at 1300 MHz and the results are shown in Table 1. These results show that we can sound 5-km thick ice with loss of 15 dB/km, if the ice-bed interface is smooth and planar reflector equations are valid for rms height deviations less than 1 cm. Our system is capable of sounding 5-km thick low-loss ice with a planar ice-bed interface and mapping internal structure. It can also sound close 5-km thick ice with a rough interface. Also the use of the array antenna configuration will allow us to generate 3-D images of the ice-bed interface and ice surface [Paden et al, 2010, Gogineni et al., 2014 and Rodriguez-Morales et al, 2014]. However, this requires a more detailed investigation during the Phase-A study.

Table 1: Radar System design and performance for planar and rough interfaces

	Planar Reflector		***Rough Interface***	
Parameter	1300 MHz		1300 MHz	
Transmit Power, PT	63.00	dBm	63.00	dBm
Antenna Gan G=45 dBi	90.00	dB	90.00	dB
Wavelength, ? ^{2} for planar ? ^{3} for rough surface	-12.74	dBm^2	-19.10	dBm^3
Two power transmission coefficient (1 -|?| ^{2})^2	-0.69	dB	-0.69	dB
Loss for 5 km thick ice (15 dB/km)	-75.00	dB	-75.00	dB
Pulse compression gain, CI	31.76	dB	31.76	dB
Integration gain, M	30.00	dB	30.00	dB
Spreading loss term -1	28.00	dB	32.98	dB
Spreading loss term -2	115.69	dBm^2	144.61	$dBm^{2.5}$
Noise power	-90.00	dBm	-90.00	dBm
Scattering coefficient	-10.00		-20.00	dB
The term from Area substitution, sqrt(cTc)/vTin			-27.16	dB
Signal-to-Noise Ratio	62.65	dB	12.39dB	

Surface clutter

One of the major challenges in orbital sounding of any sub-surface target is surface clutter, off-vertical scattered signals by the rough surface illuminated by the main beam or sidelobes of the antenna. The surface clutter can often mask weak ice-bottom returns as has been observed over fast-flowing glaciers and ice-sheet margins [Li et al. 2013; Gogineni et al. 2014]. Synthetic aperture radar (SAR) processing can be used to synthesize narrow antenna-beam with low sidelobes to reduce clutter in the along-track direction. However, SAR is ineffective for reducing clutter in the cross-track direction and it can only be achieved by using a physical antenna array. However, the size of an array that can be accommodated on an aircraft or a spacecraft is limited so advanced array processing techniques must be used as done by Li et al. [2013] and Gogineni et al. [2014] to reduce clutter. For an orbital radar operating from an altitude of 600 km, the surface

scattering from incidence angles of 5º and 7.5º can mask returns from ice beds covered with 2 and 5 km thick ice, respectively. The beamwidth of the large deployable 15-m antenna at 1300 MHz is about 1 deg. The antenna sidelobes beyond 4^0 must be less than 40 dB in the cross-track direction. This level of performance can be achieved with careful design of the feed array for the reflector antennas.

Figure 6 shows data collected with a radar sounder on NASA DC-8 aircraft flying at an altitude of about 10, 000 m above the ice surface. These radar data are collected at a center frequency of 195 MHz with a 5-element array. The echogram on top left shows SAR image generated with a sum and delay beamformer with Hanning weights. The surface is clearly visible, but bed is completely masked by the surface clutter. The echogram on the top right shows a SAR image generated using a Minimum Variance Distortionless Response (MVDR) beamformer with a clearly discernable bed [Li et al., 2013 and Van Trees, 2002]. These results in Figure 6 are the first successful demonstration of coherent clutter rejection for sounding ice from a high-altitude (^10,000 m above the surface) jet aircraft. These techniques can be applied to deal with clutter

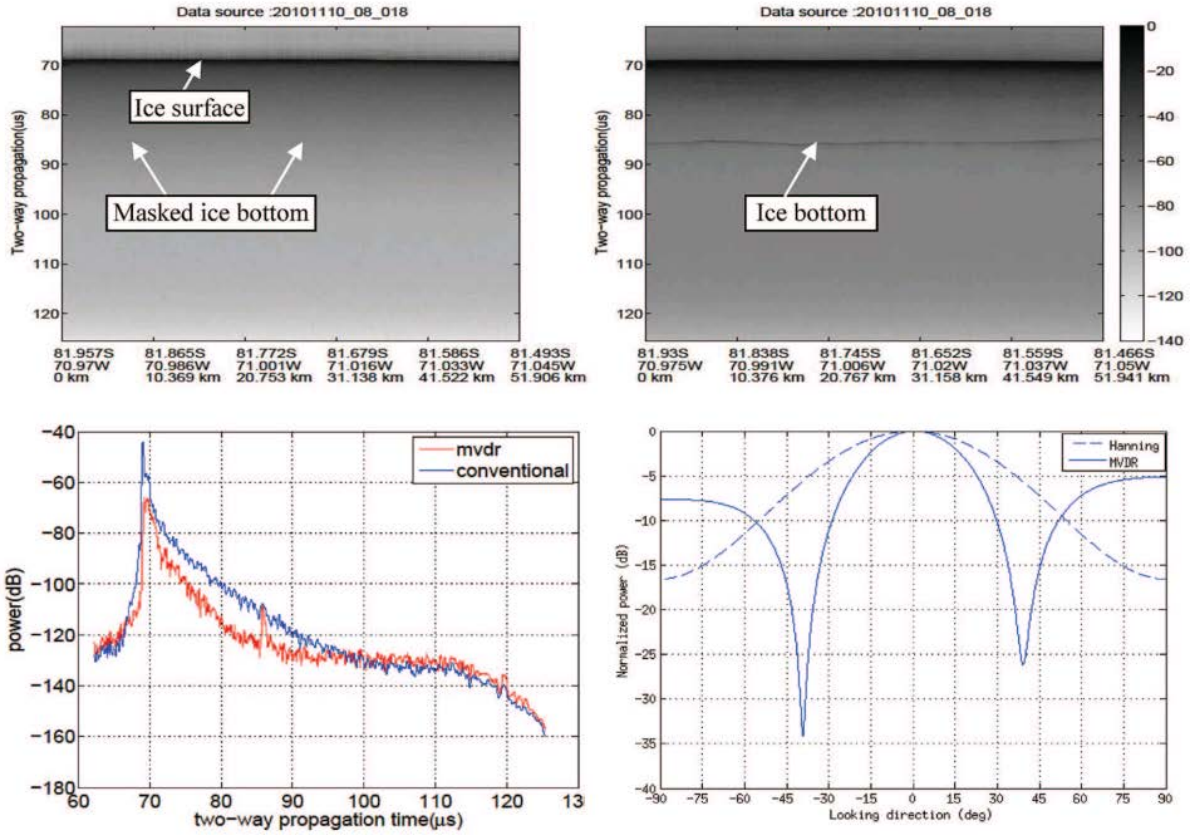

Figure 6: Effect of surface clutter and application of coherent clutter reduction algorithm to reduce clutter.

issues for our satellite-based radar to sound and image ice. The bottom left inset shows an A-scope (amplitude as a function of range) for a range-line processed with conventional and MVDR beamformers. The data processed with MVDR beamformer shows the bed return to be 10 dB above the surrounding signal. The right-bottom inset shows conventional and MVDR beamformer antenna patterns. The MVDR beamformer placed nulls at the clutter angles, similar to what we propose to do with the 1300-MHz radar sounder/imager. We propose to incorporate real-time array processor in our system to reduce clutter with the proposed 11-element array at 1300 MHz. We estimate a total clutter reduction will be more than 80 dB both in the along-track and cross-

track directions. We can use a conventional sum-delay beamformer for transmission and MVDR beamformer reception to suppress clutter.

Range sidelobes

Pulse-compression techniques must be used for long-range detection of targets typical of an orbital radar. Long-chirped or -coded pulses are transmitted to obtain the energy required to detect long-range targets and received signals are decoded or dechirped to generate a short pulse to obtain fine range resolution in a pulse compression radar. The main disadvantage of pulse compression is the resulting range sidelobes from the dechirping process. The range sidelobes exist for a time duration equal to the uncompressed pulse width on both sides of the main target peak. The range sidelobes of strong returns from the ice-surface or internal layers can mask the weak echoes from the ice-bed interface. We have already developed airborne radars with range siddelobes of 70 dB or lower by amplitude tapering the transmit waveform and windowing the received signal [Li et al., 2013; Kowatsch and Stocker, 1982; Misaridis and Jensen, 2001]. Figure 7 shows the transmit waveform shaped with a 10% Tukey window to reduce Fresnel ripples associated with rapid rise and fall times at the start and the end of a chirp. The bottom-panel shows the measured point target response with range sidelobes of 70 dB and lower. We simulated the point target using a delay line constructed with fiber-optic cable, RF-Optical transceivers and RF attenuators. We selected the length of the fiber to obtain a delay of 36 µs. The sidelobes beyond ±2 µs from the main peak are suppressed by more than 80 dB. We are confident that we can design a pulse-compression system with sidelobes of 70 dB or lower.

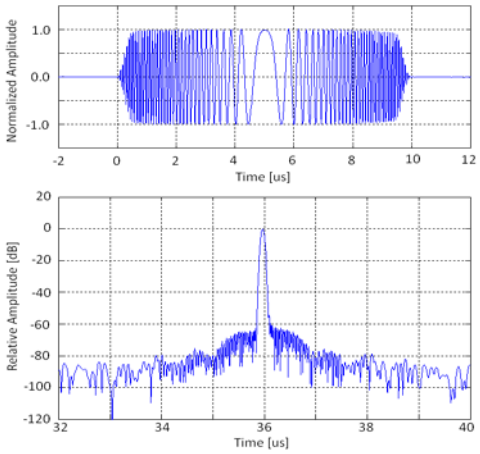

Figure 7: Top panel shows an amplitude tapered transmit LFM chirp waveform. Bottom panel shows the measured point target response simulated with a fiber optic delay line.

4.0 Satellite Systems and Configuration

The proposed satellite mission concept employs proven spacecraft systems and technology in a robust and high-precision configuration. The innovative subsystems are the radar and reflector; otherwise, the remaining satellite subsystems operate as a modern remote-sensing satellite including solar power generation, thermal regulation, station-keeping, and uplink/downlink communications.

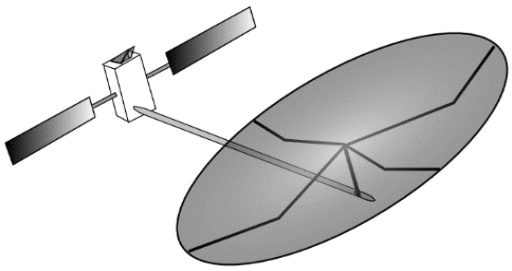

Figure 8: Conceptual structural and mission systems components: reflector, boom, radar, power generation, and attitude control.

The antenna-system consists of a 15-m reflector parabolic dish (i.e. 176 m^2 area) with an offset-feed L-band phased array mounted on the satellite bus. A conceptual systems diagram demonstrating the deployed configuration is shown in Figure 8. A 16-m multi-part deployable boom connects the reflector to the bus. The proposed configuration provides a substantial advantage in antenna efficiency since the array is directly mounted on the bus with only a minimal internal feedline to the radar system. The reflector dish is composed of unfolding support ribs and

an unfurling reflector-mesh membrane. The mesh and ribs are launched folded against the main satellite bus. The unfolding process beings with unfolding the boom from the bus, followed by unfolding of the reflector ribs, finally followed by unfurling of the mesh membrane. The critical advantages of an unfurling mesh membrane are: 1) the large surface areas of a membrane with the small launch volume; 2) a rolled rather than folded surface for the elimination of surface kinks; and 3) elastic wrapping assisted deployment for redundancy and consistency. Unfurling reflectors are a technologically mature solution to packing and space deployment. NASA has demonstrated the maturity of the technology with the Large Space System Technology (LSST) demonstration of a 55-m wrap rib antenna, [Anderson et al., 1985]. Lockheed Missiles and Space Company (LMSC) demonstrated a surface contour evaluation and adjustment system using a laser-ranging system and translation of the struts supporting the mesh.

An initial study of the launch packing and deployment process indicates a total spacecraft launch length of approximately 5 meters, a cross section diameter of 2 meters, and a mass of 900 kg. After deployment, the satellite's size is approximately 20 by 20 meters by 15 meters.

Electrical power analysis suggests solar cells and a battery system. The radar system uses an average of 400 W continuous with transients up to 2000 W for the scanning duration. Attitude Determination and Control System (ADCS) continuous power levels are estimated at 200 W. The heating system for the electronics and antenna reflector are estimated at 250 W, [Emis, 2012]. Antenna control, communications, power control, and the on-board computer will require about an average of 100 W. Overall average power draw is approximately 1 kW. Based on the transient nature of the power draw, a battery system capable of supplying up to 5 kW is necessary. Modern Ni-H_2 and Li-ion battery energy densities of 50-100 W-hr/kg suggest a battery mass in the 100 kg range. Solar cells are advantageous given the orbit profile and power requirements. Current high-power solar arrays have a specific mass of 40 W/kg and a specific volume of 8 kW/m3, [Penn, 2014]. The solar-array is initially estimated at 50 m^2. These conceptual power system estimates provide a robust and resilient satellite system with scanning and station-keeping flexibility.

With a primary target of Antarctica, a 90˚ inclination polar orbit was selected (Figure 9). The polar orbit additionally allows the scanning access to the entire Earth. A low earth orbit (LEO) of 600 km gives a 1 hour 36-minute orbital period for approximately 11 minutes over Antarctica per orbit. The polar orbit also shows advantageous properties for rapid rescanning capability. The orbital decay rate at 600 km is negligible enough for a 5-year operational period before deorbit is necessary. The launch system requires approximately ΔV=25 km/s for the 600-km altitude with a direct launch to the polar orbit. A direct launch allows for a wider range of launch rocket platforms. The launch profile allows a wide range of launch vehicles including the Ariane 5 and SpaceX's Falcon 10. The Falcon 9 fits the launch profile, volume, and mass particularly well.

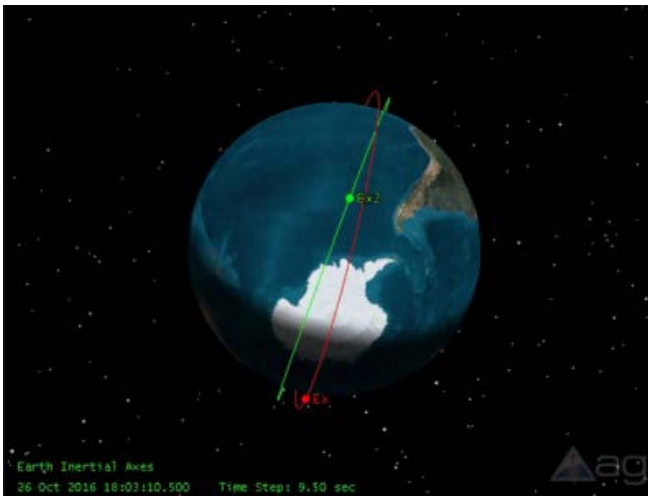

Figure 9: Orbit simulation in STK showing the high inclination polar orbit selected passing over Antarctica. Orbital period is 1 hour 36 min.

Figure 10 illustrates our concept for collecting data in normal strip-map mode for soil moisture and other applications and nadir-looking mode to sound and image ice, as well as measure bottom melt rates of ice shelves. The satellite-based radar in conjunction with a microwave radiometer can address two major issues related to climate change impacts—water resource management and accurate sea-level rise estimates needed to develop coastal protections.

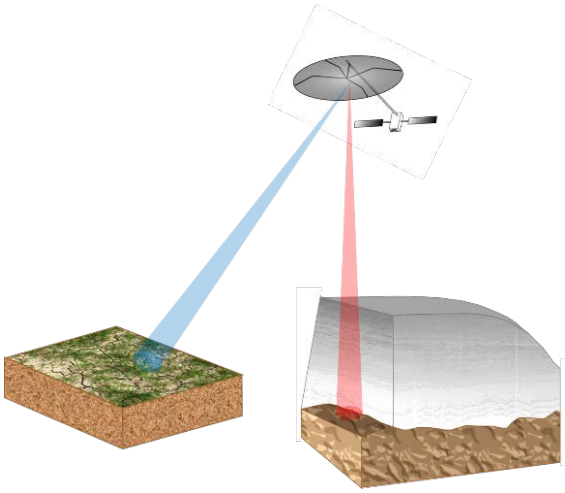

Figure 10: Conceptual illustration for operating the radar in strip-made mode for soil moisture and other related measurements, and sounding and imaging of ice.

5.0 Conclusions:

A satellite-based L-band radar with a large deployable reflector can be used for soil moisture measurements. The same radar can be used to sound and image large ice sheets in Antarctica and Greenland as well as measure bottom melt rates of ice shelves in Antarctica. The large-reflector can also be used to include a radiometer with improved resolution for soil moisture measurements and also determining ice temperature as a function of depth. We recommend a detailed study to determine the feasibility and cost of a satellite radar/radiometer mission using a large deployable reflector.

References:

1. Abdalati, W. et al., 2010. The ICESat-2 Laser Altimetry Mission. *Proceedings of the IEEE,* 98(5), pp. 735-751.
2. Anderson, G. C., Garrett, L. B., and Calleson, R. E., "Comparative Analysis of On-Orbit Dynamic Performance of Several Large Antenna Concepts," AIAA Paper 85-0818, doi: 10.2514/6.1979-932.
3. Belvin, W.K, 2004, Advances in Structures for Large Space Systems, http://ntrs.nasa.gov/archive/nasa/casi.ntrs.nasa.gov/20040139601.pdf
4. Cooper, B. J., Black, J. T., Swenson, E. D., and Cobb, R. G. "Rigidizable Inflatable Get-Away-Special Experiment (RIGEX) Space Flight Data Analysis, AIAA Paper 2009-2157, May 2009.
5. Dahl-Jensen, D. et al., Eemian interglacial reconstructed from a Greenland folded ice core. Nature 493, 489-494, doi:10.1038/nature11789 (2013).
6. Davis, G. L, and Tanimoto, R. L., "Mechanical Development of Antenna Systems," *Spaceborne Antennas for Planetary Exploration,* edited by J. H. Yuen, Deep Space Communication and Navigation Series, Jet Propulsion Laboratory, California Institute of Technology, NASA, Jan. 2006.
7. Dubois, P., van Zyl, J. & Engman, T., 1995. Measuring soil moisture with imaging radars. *IEEE Trans. Geosci. Remote Sens.,* 33(4), pp. 915-926.
8. Emis, N., Kwack, E., Mikhaylov, R., Lau, D., Miller, J., and Cucullu, G., "Design Overview of the Thermal Control System for the SMAP Mission," TFAWS Passive Thermal Paper Session, Thermal & Fluids Analysis Workshop, Aug. 13-17 2012.
9. Entekhabi, D., et al., "The Hydrosphere State (HYDROS) mission concept: An earth system pathfinder for global mapping of soil moisture and land freeze/thaw," IEEE Trans. Geosci. Remote Sens., vol. 42, no. 10, pp. 2184-2195, Oct 2004.
10. Entekhabi, D., et al., "The Soil Moisture Active Passive (SMAP) Mission," Proceedings of the IEEE, vol. 98, no. 5, pp. 704-716, May 2010.
11. Flowers, G. E., 2015. Modelling water flow under glaciers and ice sheets. *Proc. R. Soc. A,* 471(2176).
12. Freeland, R. E., "Significance of the Inflatable Antenna Experiment Technology," AIAA Paper 98-2104, doi: 10.2514/6.1998-2104.
13. Fujita, S. et al., 2000. A summary of the complex dielectric permittivity of ice in the megahertz range and its applications for radar sounding of polar ice sheets. *Physics of Ice Core Records,* pp. 185-212.
14. Gagliardini, O. et al. Capabilities and performance of Elmer/Ice, a new-generation ice sheet model. Geoscientific Model Development 6, 1299-1318, doi:10.5194/gmd-6-1299-2013 (2013).
15. Gaspar, J. L., Mann, T., Sreekantamurthy, T., and Behum, V., "Structural Test and Analysis of a Hybrid Inflatable Antenna," AIAA Paper 2007-1832, April 2007.
16. Gogineni, S. et al. Polar radar for ice sheet measurements (PRISM). Remote Sensing of Environment 111, 204-211, doi:10.1016/j.rse.2007.01.022 (2007).
17. Gogineni, P., J. Li, J. Paden, R. Crowe, A. Hoch, C. Lewis, E. Arnold, F. Rodriguez-Morales, C. Leuschen, R. Hale, A.R. Harish, and D. Braaten (2012), "Sounding and

Imaging of Fast Flowing Glaciers and Ice-Sheet Margins," EUSAR 2012, April 23-26, Nuremberg, Germany, 2012.
18. Gogineni, P., J.B. Yan, R. Hale, C. Leuschen, F. Rodriguez-Morales, Z. Wang, J. Paden, B. Townley, D. Gomez-Garcia, L. Stearns, C. Carabajal, R. Willer and S. Child (2014), "Ultra-Wideband Radar for Measurements over Ice Sheets in Antarctica and Greenland," EUSAR 2014, June 3-5, Berlin, Germany, 2014A.
19. Gogineni, S., J.-B. Yan, J. Paden, C. Leuschen, J. Li, F. Rodriguez-Morales, D. Braaten, K. Purdon, Z. Wang, W. Liu and J. Gauch, 2014. "Bed topography of Jakobshavn Isbrae, Greenland, and Byrd Glacier, Antarctica," Journal of Glaciology, Vol. 60, No. 223, 813-833, September 2014B.
20. Gudmundsson, G. H., Krug, J., Durand, G., Favier, L. & Gagliardini, O. The stability of grounding lines on retrograde slopes. Cryosphere 6, 1497-1505, doi:10.5194/tc-6-1497-2012 (2012).
21. Howat, I.M., I. Joughin, and T.A. Scambos, Rapid changes in ice discharge from Greenland outlet glaciers. Science 315, 1559-1561, 2007.
22. IPCC, "Climate Change 2014: Synthesis Report, Contribution of Working Groups I, II and III to the Fifth Assessment Report of the Intergovernmental Panel on Climate Change," Geneva, Switzerland.
23. Jevrejeva, Grinsted, Moore (2014), Upper limit for sea level projections by 2100, Environ. Res. Lett. 9 104008 doi:10.1088/1748-9326/9/10/104008
24. Joughin, I., R. Kwok, and M. Fahnestock , Estimation of ice-sheet motion using satellite radar interferometry: Method and error analysis with application to Humboldt Glacier, Greenland, J. Glaciol., 42(142), 564-575, 1996
25. Joughin, I.,W. Abdalati, and M. Fahnestock , Large fluctuations in speed on Greenland's Jakobshavn Isbræ glacier, Nature, 432, 608–610, 2004.
26. M. Kowatsch and H. R. Stocker. Effect of Fresnel ripples on sidelobe suppression in low time-bandwidth product linear FM pulse compression. IEE Proc., 129:41–44, 1982.
27. Yann H. Kerr, Philippe Waldteufel, Philippe Richaume,Jean Pierre Wigneron,, Paolo Ferrazzoli,Ali Mahmoodi, Ahmad Al Bitar, François Cabot, Claire Gruhier, Silvia Enache Juglea,Delphine Leroux, Arnaud Mialon, and Steven Delwar, The SMOS Soil Moisture Retrieval Algorithm, IEEE TRANSACTIONS ON GEOSCIENCE AND REMOTE SENSING, VOL. 50, NO. 5, MAY 2012.
28. Delphine J. Leroux ; Narendra Narayan Das ; Dara Entekhabi ; Andreas Colliander ; Eni G. Njoku ; R. Scott Dunbar ; Simon H., Active–Passive Disaggregation of Brightness Temperatures During the SMAPVEX12 Campaign**,** IEEE Transactions on Geoscience and Remote Sensing, Volume: 54, Issue: 12, Dec. 2016.
29. Lewis C, Gogineni P, Rodriguez-Morales F, Panzer B, Stumpf T, Paden J, and Leuschen C (2015) Airborne UHF Radar for Mapping Near Surface Internal Layers and Measuring Shallow Ice Thickness. Journal of Glaciology, 61(225), 89-100.
30. Lewis, C., Ice Shelf Melt Rates and 3D Imaging, Ph.D. Dissertation, The University of Kansas, 2015,
31. Li, J., J. Paden, C. Leuschen, F. Rodriguez-Morales, R. Hale, E. Arnold, R. Crowe, D. Gomez-Garcia and P. Gogineni, 2013. "High-Altitude Radar Measurements of Ice

Thickness over the Antarctic and Greenland Ice Sheets as a part of Operation Ice Bridge," IEEE Trans Geosci. Rem Sens., Volume 51, Issue 2, 742-754, February 2013.
32. Li, X., Rex J. Rowley, John C. Kostelnick, David Braaten, Joshua Meisel, and Kalonie Hulbutta, GIS Analysis of Global Impacts from Sea Level Rise, Photogrammetric Engineering & Remote Sensing Vol. 75, No. 7, July 2009, pp. 807–818.
33. Mathers, N. M., and Thompson, L. A., "Inflatable Antennas in Terrestrial and Extraterrestrial Environments," IAC Paper 06-B3.2.05, Mar. 2005.
34. T. Misaridis and J. Jensen, "Use of modulated excitation signals in medical ultrasound, part II: Design and performance for medical imaging applications," IEEE Trans. Ultrason., Ferroelectr., vol. 52, no. 2, pp. 192–207, Feb. 2005
35. Moore, R. K. and S. Gogineni, "Large Space Antenna Technology Applied to Radar Imaging, Rain-Rate Measurements, and Ocean Wind Sensing," NASA Conference Publication #2368, pp. 97-108, 1984.
36. NASA JPL, 2015. [Online] Available at: http://www.jpl.nasa.gov/news/news.php?feature=4710
37. NI-SAR Workshop Report, 2014, http://www.sac.gov.in/nisar/NISAR%20Science%20Workshop_Report-2014.pdf
38. NOAA, "Billion-Dollar Weather and Climate Disasters: Table of Events", 2016, http://www.ncdc.noaa.gov/billions/events
39. Paden, J., T. Akins, D. Dunson, C. Allen, and P. Gogineni, "Ice-sheet bed 3-D tomography," Journal of Glaciology, Volume 56, Number 195, pp. 3-11, January 2010.
40. R. Panciera, J. Walker, T. J. Jackson, D. Ryu, D. Gray, A. Monerris, H. Yardley, M. Tanese, C. Rudiger, X. Wu, Y. Gao, and J. Hacker, Soil Moisture Active Passive Experiments (SMAPEx): Towards soil moisture retrieval from the SMAP mission , IEEE Journal of Selected Topics in Earth Observations and Remote Sensing , 51, no. 1, pp. 490–507; 2014
41. Pattyn, F., et al., Benchmark experiments for higher-order and full Stokes ice sheet models (ISMIP- HOM), The Cryosphere Discuss., 2, 111–151, 2008.
42. Penn, J. P., Mayberry, J. P. Ranieri, C. L., and Rossi, O. K., "Re-Imagining SMC's Fleet with High Power Solar Arrays and Solar Electric Propulsion," AIAA Paper 2014-4328, Aug. 2014.
43. Pritchard, H.D., Arthern, R.J., Vaughan, D.G., and Edwards, L.A., "Extensive dynamic thinning on the margins of the Greenland and Antarctic ice sheets," Nature, 2009. [Online] doi: 10.1038/nature08471
44. Rignot, E. and P. Kanagaratnam, "Changes in the Velocity Structure of the Greenland Ice Sheet". Science 311 (5763): 986-990, 2006.
45. Rignot, E., Mouginot, J., Morlighem, M., Seroussi, H., and Scheuchl, B., "Widespread, rapid grounding line retreat of Pine Island, Thwaites, Smith, and Kohler glaciers, West Antarctica, from 1992 to 2011," Geophys. Res. Lett., 41, 3502-3509, 2014. doi:10.1002/2014GL060140.
46. Rodriguez-Morales, F. et al., 2014. Advanced multifrequency radar instrumentation for polar research. *IEEE Transactions on Geoscience and Remote Sensing*, 52(5), pp. 2824-2842.

47. Rowley, R. J., J. C. Kostelnick, D. Braaten, X. Li, and J. Meisel. 2007. Risk of rising sea level to population and land area. 2007. EOS Transactions 88(9) (27 February 2007): 105, 107.
48. Russell, R. A., Campbell, T. G., Freeland, R. E., "A Technology Development Program for Large Space Antennas," NASA-TM-81902, IAF-80-A-33, Sep. 1980.
49. Shepherd, A. et al., "A Reconciled Estimate of Ice Sheet Mass Balance," Science, vol. 338, no. 6111, pp. 1183:1189, doi: 10.1126/science.122 8102, 2012.
50. Shi, J. et al., 2014. *WCOM: The science scenario and objectives of a global water cycle observation mission.* Quebec City, QC, s.n., pp. 3646-3649.
51. Shi, J. et al., 1997. Estimation of bare surface soil moisture and surface roughness parameter using L-band SAR image data. *IEEE Trans. Geosci. Remote Sens,* 35(5), pp. 1254-1266.
52. Sorensen, L. S. et al. Mass balance of the Greenland ice sheet (2003-2008) from ICESat data - the impact of interpolation, sampling and firn density. Cryosphere 5, 173-186, doi:10.5194/tc-5-173-2011 (2011).
53. Smith, T.T., BF Zaitchik, and JM Gohlke (2013) Heat waves in the United States: definitions, patterns and trends. Climatic Change. DOI 10.1007/s10584-012-0659-2
54. Stumpf, T. A Wideband Direction of Arrival Technique for Multibeam, Wide-Swath Imaging of Ice Sheet Basal Morphology. CReSIS Technical Report, Lawrence, KS, University of Kansas 163, 125 (2015).
55. Suzuki, Y., Harada, S., Kobayashi, K., Ueba, M., and Ohara, K., "Deformed Antenna Pattern Compensation Method for onboard Multi-beam Antennas," AIAA Paper 2007-3269, April 2007.
56. Van Trees, H. L, Optimum Array Processing: Part IV of Detection, Estimation, and Modulation Theory, John Wiley & Sons, Inc., 2002.
57. Weertman, J., 1957. On the sliding of Glaciers. *Journal of Glaciology,* pp. 33-38.
58. Zhao, T. and A. Dai, 2015. The magnitude and causes of global drought changes in the Twenty-First Century under low-moderate emissions scenario, Journal of Climate, 28, 4490-4512.
59. Zwally, H.J. et al., "Mass changes of the Greenland and Antarctic ice sheets and shelves and contributions to sea- level rise: 1992-2002," Journal of Glaciology, 51(175), 509-527, 2005.